Nonlinear fibre element modelling of RC bridge piers considering inelastic buckling of reinforcement

Mohammad M Kashani[1], Laura N. Lowes[2], Adam J Crewe[3], Nicholas A. Alexander[4]

Abstract

An advanced modelling technique is developed to model the nonlinear cyclic response of circular RC columns using fibre-based section discretisation method. A comparison between different reinforcing steel models is made. Through a comprehensive parametric study the influence of inelastic buckling of vertical reinforcement on the cyclic response of circular RC columns is investigated. The results have been compared and validated against a set of experimental datasets. The proposed calibrated model accounts for the influence of inelastic buckling of vertical reinforcement and interaction of stiffness of horizontal ties reinforcement with vertical reinforcement. The model also accounts for the fracture of vertical bars due to low-cycle high-amplitude fatigue degradation. Therefore, this model is able to predict the nonlinear cyclic response of circular RC columns up to complete collapse. The results show that the existing uniaxial material models of reinforcing bars that are calibrated using stress-strain behaviour of isolated bars cannot represent the behaviour of reinforcing bars inside RC columns. Moreover, it is found that the buckling length of vertical reinforcement has a significant influence on the pinching response of RC columns and also reduces the low-cycle fatigue life of buckled reinforcement.

Keywords: Nonlinear analysis, Finite element method, Reinforcing steel, Buckling, Force-based element, Postbuckling, Reinforced concrete, Bridge piers, Low-cycle fatigue, Cyclic degradation

1. Introduction

Modern bridge design practice has improved the seismic response of bridges under earthquake loading when compare to the older bridges. Nevertheless the earthquake damage is expected and has been observed in the recent large earthquakes. Even bridges which suffer minor

[1]Lecturer, University of Bristol, Dept. of Civil Engineering University of Bristol, Bristol, BS8 1TR, United Kingdom (corresponding author), E-mail: mehdi.kashani@bristol.ac.uk
[2]Associate Professor, University of Washington, Dept. of Civil and Environmental Engineering University of Washington, Seattle, WA 98195-2700, United States of America
[3]Reader, University of Bristol, Dept. of Civil Engineering University of Bristol, Bristol, BS8 1TR, United Kingdom
[4]Senior Lecturer, University of Bristol, Dept. of Civil Engineering University of Bristol, Bristol, BS8 1TR, United Kingdom

damage after the earthquake require post-earthquake repair and result in a significant cost to bridge owners. To this end, it is very important for bridge owners and managers to be able to predict the earthquake damage on their bridges. This will help to improve the whole life cycle cost (WLCC) analysis of bridges. The existing performance-based earthquake engineering (PBEE) relates the economic impact to the structural damage for a given hazard level. Therefore, it requires response models to predict the seismic demand of reinforced concrete (RC) bridges under multiple hazard levels, and damage models to predict the corresponding damage state. Finally PBEE framework links the column demands with damage state to estimate the economic loss. Accordingly, several researchers have studied the trends between the demand parameters (e.g. drift ratio or strain at critical sections) and damage parameters (e.g. bar buckling) experimentally [1-3].

Moreover, recent advances in computational tools have enabled researchers to use refined modelling techniques in the analyses. This has improved the modelling nonlinear behaviour of structures and bridges subject to earthquake loading. The fibre-based finite element technique [4-6], is the most recent and popular method for nonlinear analysis of framed structures. In this method element cross section is discretised into a number of fibres at the selected locations along the length of element known as "integration points". The behaviour of each fibre is modelled by a uniaxial nonlinear material model. Reinforcing steel, unconfined cover concrete and core confined concrete are treated as separate material models at section level. Therefore, the component response is primarily controlled by inelastic response of the cross section. Accordingly, several researchers have developed uniaxial material models to be used in fibre-based finite element models.

As it is well known to researchers, buckling of vertical reinforcement in RC columns is the most common type of observed failure mechanism [1-3]. Despite the significant efforts in the past two decades or so in development of buckling models for reinforcing bars and simulation of buckling of reinforcing bars in RC columns [7-25], there is still not a precise model that has been extensively validated against experimental datasets. To this end, there are two major concerns about the existing models: *i*) all of the existing models are calibrated based on either experimental and/or numerical stress-strain behaviour of isolated bars that may or may not represent the actual behaviour of embedded reinforcing bars inside concrete, *ii*) the stress-strain behaviour of reinforcing bars is averaged over the buckling length. Therefore, consideration needs to be given to the element mesh size that will affect the integration scheme of fibre model. Ignoring this phenomenon will result in strain localisation at the critical section [26,27].

Kashani [28,29] developed a new phenomenological uniaxial material model that accounts for the effect of inelastic buckling, low-cycle fatigue degradation and long-term corrosion damage on hysteretic behaviour of isolated reinforcing bars. This model has been implemented to the OpenSees [30] (an open source finite element computer code) as a new uniaxial material class, called *CorrodedReinforcingSteel* material model. If the percentage mass loss (measure of corrosion damage) in the material input parameters is taken as zero the model represents stress-strain behaviour of the uncorroded reinforcement.

This paper presents a comparison between the new *CorrodedReinforcingSteel* and the existing *Steel02* available in the OpenSees. The discussion of *Steel02* and other uniaxial material models used in the analyses is available in section 5 of this paper. Moreover, the material parameters of *CorrodedReinforcingSteel* have been calibrated for circular RC column through a comprehensive parametric study. The objectives of this paper are:

i) to calibrate material parameters of the *CorrodedReinforcingSteel* model for circular RC columns to account for the interaction of tie reinforcement and vertical reinforcement.

ii) to predict the impact of bar buckling on cyclic degradation, strength loss and failure mode of flexural govern RC columns.

iii) to develop an advanced computational modelling technique for simulation of bar buckling in RC columns.

2. Experimental RC bridge column dataset

The University of Washington-Pacific Earthquake Engineering Research Centre (UW-PEER), experimental test database [31] is an important repository of the nonlinear performance of the RC columns. This data set enables the calibration of the numerical model parameters. The database documents columns geometry, material properties, and reinforcement details. It also includes the force-displacement histories, and the observed drift at the onset of different damage states. For this study ten of the buckling critical column experiments are considered for model validation and calibration. Table 1 summarises the details of the selected columns and their references. In Table 1, L is the column length, L/D ratio is column length to column diameter ratio, ρ_l is the ratio of longitudinal reinforcement area to total cross sectional area, ρ_h is the volumetric ratio of horizontal reinforcement and $P / (A_g f_c)$ is the axial force ratio, where P is the axial force on the column, A_g is the gross cross section area of column and f_c is the

compressive strength of concrete. The details of material properties can be found in either UW-PEER column data base or in the relevant reference that is shown in Table 1.

Table 1 details of column dataset

ID	Reference	L (mm)	L/D	ρ_l (%)	ρ_h (%)	Axial Force ratio, $P/(A_g f_c)$
(1)	Kunnath et al. A2 [32]	1372	4.5	2.04	0.01	0.09
(2)	Lehman and Moehle 415 [33]	2438.4	4	1.49	0.01	0.07
(3)	Lehman and Moehle 815 [33]	4876.8	8	1.49	0.01	0.07
(4)	Lehman and Moehle 1015 [33]	6096	10	1.49	0.01	0.07
(5)	Lehman and Moehle 407 [33]	2438.4	4	0.75	0.01	0.07
(6)	Lehman and Moehle 430 [33]	2438.4	4	2.98	0.01	0.07
(7)	Henry 415p [33]	2438.4	4	1.49	0.01	0.12
(8)	Henry 415s [33]	2438.4	4	1.49	0.00	0.06
(9)	Moyer and Kowalsky 1[34]	2438.4	5.33	2.08	0.01	0.04
(10)	Hamilton UCI1 [35]	1854.2	4.6	1.17	0.01	0.00
	Mean	2882.9	5.24	1.65	0.01	0.07
	Standard Deviation	1372.1	1.97	0.57	0.00	0.03
	Max	6096.0	10.00	2.98	0.01	0.12
	Min	1372.0	4.00	0.75	0.00	0.00

3. Finite element model of RC bridge piers using nonlinear fibre beam-column element

There are two methods of element formulation to formulate distributed plasticity frame models such as displacement-based and force-based formulations [4]. In the displacement-based formulation, the displacement vector fields along the element are expressed as functions of the nodal displacements. The assumed displacement fields are approximations of the actual displacement fields, and therefore several elements per member are required to obtain a good approximation of the exact response. In the force-based formulation, the internal force fields are expressed as functions of the nodal forces [4-6].

A fibre beam-column element is a line element in which the moment-curvature response at selected locations (along the element known as integration points) is determined from the fibre section assigned to that integration point. Currently, forced-based (also known as flexibility-based) fibre element is the most advanced one dimensional element for nonlinear analysis of RC components. In flexibility-based elements the curvatures at each integration point are estimated for the given moment at that section. Finally, the element response is obtained through weighted integration of the sections response [4]. In RC beams and columns usually inelastic behaviour occurs near the end of the component (plastic hinge region). Therefore, the

Gauss-Lobatto integration scheme, in which the integration points are placed at the ends of the element, as well as along the column length, is recommended [36].

Force-based elements are well suited for nonlinear analysis of framed structures because they allow the spreading of plasticity over the length of the member using only one element that has multiple integration points. However, it is well known that forced-based elements can lose their objectivity at a local and/or global level depending on section hardening/softening behaviour [26,27]. [26] proposed a simple material regularisation technique to solve this problem. The proposed material regularisation technique is based on the observed failure mode of concrete cylinders in compression tests. In compression tests the damage is a localised phenomenon, and there is experimental evidence that the energy dissipated by concrete crushing in compression a failure (dissipated energy) is constant and independent of the length of the specimen [37,38]. [27] successfully employed this method to predict the nonlinear cyclic response of RC shear walls using force-based fibre beam-column elements. Using this concept the constitutive material model must be modified based on the integration length for the critical section to avoid this localisation problem. In RC columns where the failure mode is buckling of vertical reinforcement, softening response of the critical section is controlled by the post-buckling softening response of uniaxial material model of reinforcing steel. Therefore, the post-buckling response of reinforcing steel has significant impact on strain localisation at the critical section.

In this research, a different method is employed to avoid the strain localisation due to the post-buckling response of reinforcing bars. It is known that the uniaxial material model including the post-buckling response of reinforcing bars is averaged over a known buckling length. Given it is expected that the buckling will occur at the first critical section of the column, the integration length of this section should be considered to be equal to the buckling length.

The Gauss-Lobatto integration scheme doesn't allow adjusting the length of the first integration point to be equal to the buckling length using one force-based element for the entire column. Therefore, in this research two force-based elements are used to model the RC column. It should be noted that this is different from the conventional lumped plasticity/plastic hinge method. Although the length of the first integration point is set to be equal to buckling length, the plasticity is not limited to this location. In the lumped plasticity method, a plastic hinge length must be known. Therefore, the plasticity is forced to occur at this location. It should also be noted that the buckling length is different from plastic hinge length. Therefore, in the

proposed method in this paper, there is no need for choosing any plastic hinge in advance. It is a generic method and is valid for any case.

The proposed method employs three integration points (using Gauss-Lobatto integration scheme) for the first element. Based on the recommendation provided by [26, 27], the total length of 6 L_{eff} where L_{eff} is the buckling length (L_{eff} is defined in the section 4 of this paper) is considered for this element. This makes the length of the first integration point to be equal to L_{eff}. Using this method the length of the first element at the bottom of the column is adjusted based on the buckling length for each column. Based on the recommendations reported by [36] a forced-based element with five integration points is considered for the second element to model the top part of the column. A schematic view of the fibre model and fibre sections is shown in Fig. 1 below. The numbers of fibres and the section and discretisation method are based on the recommendations reported by [36]. To model the strain penetration and the slippage of reinforcement anchored to the foundation a zero length section element available in the OpenSees is used. The detailed discussion of the zero length section is available in section 5.4.

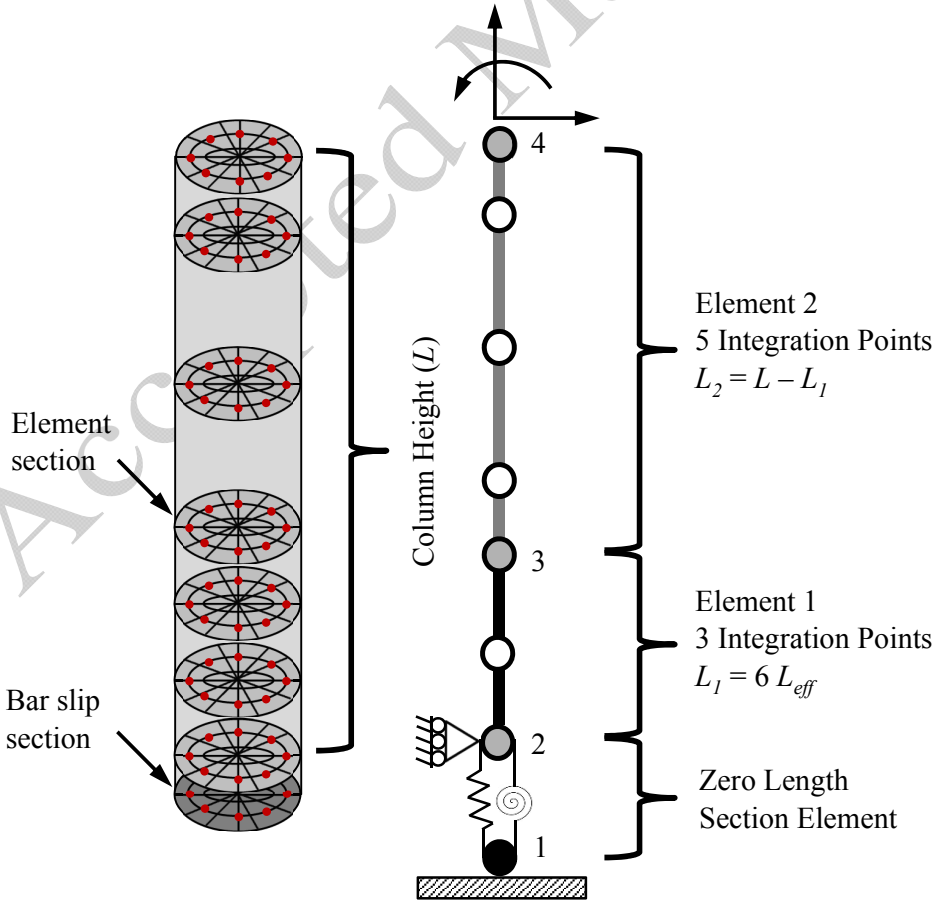

(a)

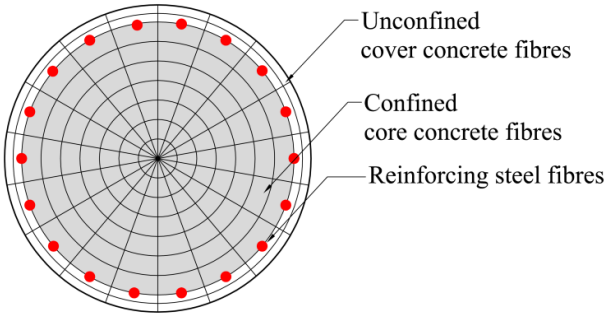

(b)

Fig. 1 Implementation of fibre beam-column element with bar buckling and bar slip model

A displacement control with an adaptive solution algorithm code is developed using the *Tcl* code in the OpenSees to run the nonlinear analysis. To check the solution convergence, the norm of displacement increment is check against a defined tolerance. This command is implemented in the OpenSees to construct a convergence test which uses the norm of the left hand side solution vector of the matrix equation to determine if convergence has been reached. The tolerance considered is 10^{-8} over the maximum of 35 iterations. The analysis starts with Newton-Raphson solution algorithm. If the convergence is not achieved the displacement increment is cut by a factor of 0.1.If the convergence is not achieved again the displacement increment is cut by another factor of 0.1. Finally if the convergence is not achieved by cutting the step sizes twice, then the solution algorithm is changed. The solution algorithms used in the adaptive solution strategy in this study includes Newton-Raphson, modified Newton-Raphson, Newton-Raphson with Line Search and Krylov-Newton algorithms. Further details of algorithm commands are available in [30].

4. Calculation of buckling length of the vertical reinforcement in circular columns

Pantazopolou [7] studied a database of column tests to identify the parameters that influence bar buckling. They concluded that the interaction between horizontal tie stiffness and spacing and bar diameter of the reinforcement influences the instability of the vertical reinforcement in columns. Based on this study, Pantazopolou [7] derived an empirical equation to calculate the buckling length of reinforcement as a function of tie stiffness.

Dhakal and Maekawa [16] studied the buckling behaviour of vertical reinforcement in rectangular columns. Using energy method, they derived the buckling mode shape accounting for the influence of tie stiffness on buckling length. This model was used in finite element

analysis of a cantilever column that was subjected to lateral and axial loads. The results of this model agreed fairly well with experimental results. However, Dhakal-Maekawa model has not been validated for circular columns. In this paper, the proposed Dhakal-Maekawa model has been used to calculate the buckling length of the experimental dataset presented in Table 1 and the result of analyses are compared with the observed experimental results.

The proposed Dhakal-Maekawa model is shown in Fig. 2. The vertical reinforcing bar is considered as a beam fixed at both ends of the buckling length to emulate the restraining mechanism of horizontal ties. A cosine shape function satisfying the fixed boundary condition is then employed to define the deformed configuration of the buckled bar.

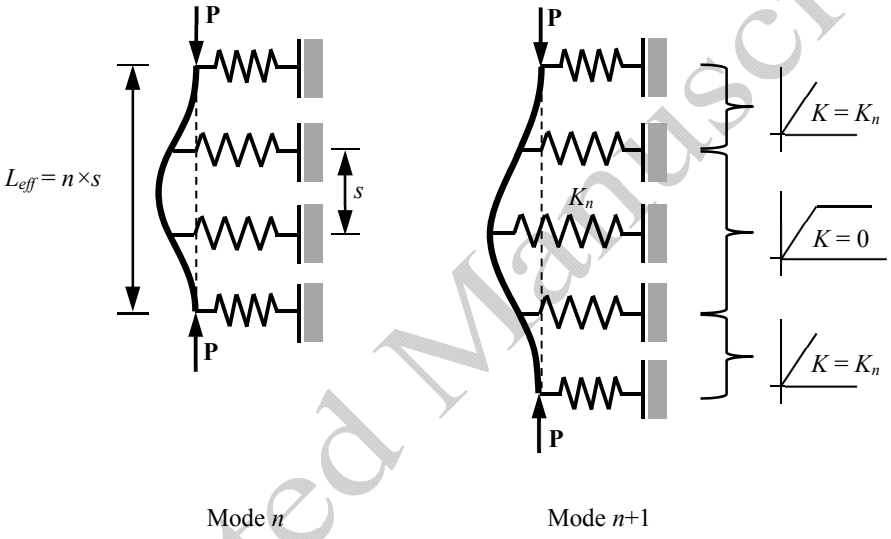

Fig. 2 Dhakal-Maekawa bar buckling model

Given the buckling of reinforcing bars is an inelastic buckling phenomenon, the elastic flexural rigidity E_sI cannot be used here [40]. Dhakal-Maekawa suggested an average flexural rigidity EI, defined in Eq. (1), which has been validated against an extensive set of experimental data.

$$EI = \frac{E_s I}{2}\sqrt{\frac{\sigma_y}{400}} \tag{1}$$

Where, E_s and σ_y are the elastic modules and yield strength of the vertical reinforcement in MPa respectively.

In this study the stiffness of horizontal ties (spiral reinforcement in circular columns) is computed using the empirical Eq. (2) suggested by Pantazopolou [7].

$$K_t = \frac{4E_{sp}A_{sp}}{\sqrt{\left(s^2 + d_c^2\right)}} \tag{2}$$

Where, E_{sp} is the elastic modulus of spiral reinforcement, A_{sp} is the cross section area of spiral reinforcement, s is the spiral pitch and d_c is the core diameter.

In the buckling model, the horizontal ties are simulated by discrete elastic springs. Based on the experimental observation it is evident that the lateral ties show elasto-plastic behaviour and their tangent stiffness is almost zero after yielding. Therefore, the stiffness of horizontal ties in the middle is considered to be zero.

Using energy method, Dhakal-Maekawa proposed an iterative procedure to calculate the required stiffness to sustain buckling mode n^{th}. Solving the Eq. (3) and Eq. (4) simultaneously yields the required spring stiffness k_n and the corresponding load P_n.

$$\frac{2\pi^4 EI}{n^3 s^3} + \sum_{i=1}^{n} \frac{c_i K_n}{4} \left(1 - \cos\frac{2i\pi}{n}\right)^2 - \frac{P_n \pi^2}{2ns} = 0 \tag{3}$$

$$\frac{2\pi^4 EI}{(n+1)^3 s^3} + \sum_{i=1}^{n+1} \frac{c_i K_n}{4} \left(1 - \cos\frac{2i\pi}{n+1}\right)^2 - \frac{P_n \pi^2}{2(n+1)s} = 0 \tag{4}$$

where, EI is the averaged flexural stiffness (Eq. (1)), s is the horizontal tie spacing and n is the buckling mode. The details and derivation of the equations are available in [16]. A flowchart of the iteration procedure is shown in Fig. 3 below.

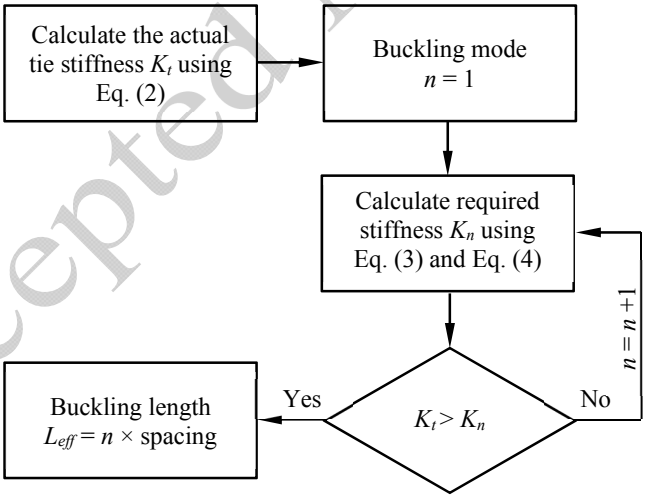

Fig. 3 iterative procedure of buckling length calculation [16]

4.1. Comparison of the computed buckling mode with observed experimental results

Using the procedure outlined in Section 4 the buckling lengths of the vertical reinforcement in the experimental dataset presented in Table 1 is computed and verified. The comparison of the computed and observed experimental results is summarised in Table 2.

Table 2 Comparison of the computed buckling mode with experimental dataset

ID*	Bar diameter d (mm)	Yield strength σ_y (MPa)	Normalised flexural rigidity EI / E_sI	Spiral pitch s (mm)	Spiral diameter d_s (mm^2)	Buckling mode computed	Buckling mode observed	s/d	L_{eff}/d
1	9.5	448.00	0.529	19	4	4	4	2	8
2	15.875	461.97	0.537	31.75	6.4	5	6	2	10
3	15.875	461.97	0.537	31.75	6.4	5	6	2	10
4	15.875	461.97	0.537	31.75	6.4	5	6	2	10
5	15.875	461.97	0.537	31.75	6.4	5	5	2	10
6	15.875	461.97	0.537	31.75	6.4	5	6	2	10
7	15.875	462.00	0.537	31.75	6.4	5	5	2	10
8	15.875	462.00	0.537	63.5	6.4	2	2	4	8
9	19.05	565.37	0.594	76.2	9.5	1	1	4	4
10	12.7	458.50	0.535	31.75	4.5	4	NA	2.5	10

* The ID number is the number allocated to the each experiment in Table 1

Based on this comparison, it is evident that Dhakal-Maekawa buckling model is in good agreement with the experimental results. Therefore the computed buckling length is used in the analyses throughout this paper.

5. Description of uniaxial material models

5.1. Concrete model

In this study the uniaxial material *Concrete04* available in the OpenSees is used in the analyses. This model is using Popovics curve [41] in the compression and a linear-exponential decay curve in tension. For unloading and reloading in compression, the Karsan-Jirsa model [42] is used to account for stiffness degradation and determine the unloading/reloading stiffness. The secant stiffness is used to define the unloading/reloading stiffness in tension. *Concrete04* is employed to model the unconfined concrete behaviour in cover concrete and a confined concrete in core concrete. The confined concrete is modelled using the confinement parameters developed by Mander et al. [43]. Fig. 4(a) shows the confined and unconfined concrete models with unloading-reloading cycling rules. Fig. 4(b) shows the concrete model in tension with unloading-reloading cycling rules. It should be noted that in Fig. 4, the σ_c is the maximum concrete compressive strength, ε_{c0} is the strain at maximum compressive strength (σ_c) and ε_{ct} is the strain at concrete fracture in tension.

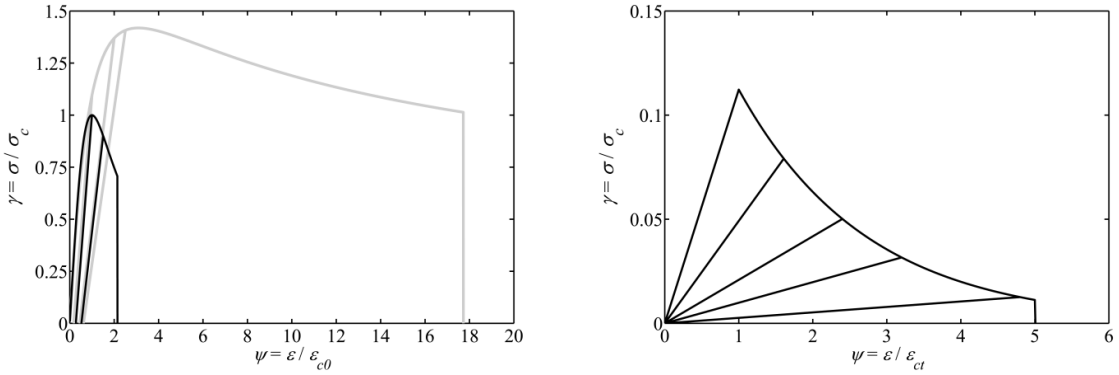

(a) **(b)**

Fig. 4 Cyclic response of concrete model employed in the analyses: (a) unconfined and confined concrete response in compression including cyclic response (b) tension response

5.2. Reinforcing steel model

5.2.1. Uniaxial reinforcing steel material model without buckling

The cyclic response of this reinforcing steel material model is defined by the Giuffre-Menegotto-Pinto (GMP) equations [44] which have been modified by Fllipou [45]. This model is available in the OpenSees known as *Steel02* uniaxial material model. The *Steel02* accounts for the Bauschinger effect [46], but does not account for cyclic strength and stiffness degradation due to bar buckling and fatigue. The only required parameters to define the *Steel02* are yield strength, elastic modulus and hardening ratio of the reinforcing steel. The cyclic response of *Steel02* is shown in Fig. 5. This model is used for the initial analyses as benchmark for comparison of the influence of cyclic degradation on inelastic response prediction models.

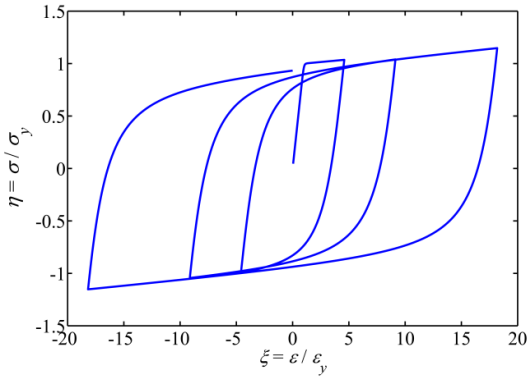

Fig. 5 Cyclic response of *Steel02* material model

5.2.2. Uniaxial reinforcing steel material model including inelastic buckling

Khashani [28] developed an advanced phenomenological uniaxial material model for reinforcing bars. The model is calibrated using experimental modelling of uncorroded and

corroded isolated reinforcing bars [19,20,28,29]. The post-buckling envelope of this model is a function of a compound non-dimensional slenderness ratio λ_p (Eq. (5)) which was originally proposed by Dhakal-Maekawa [17].

$$\lambda_p = \sqrt{\frac{\sigma_y}{100}}\frac{L_{eff}}{d} \tag{5}$$

where, L_{eff} is the calculated buckling length, d is the diameter of reinforcing bar and σ_y is the yield strength.

The influence of inelastic buckling on stiffness degradation and pinching response of reinforcing bars in compression and low-cycle fatigue degradation in tension is considered in the model. The unloading stiffness degradation in tension is also considered in the model using the model proposed by Dodd and Restrepo-Posada [47]. This model is implemented to the OpenSees as a new material class called *CorrodedReinforcingSteel*. The detailed description of this model is available in [28,29]. This model works for both corroded and uncorroded steel. An example cyclic response of this model for a reinforcing bar with L_{eff}/d = 10 and zero corrosion is shown in Fig. 6.

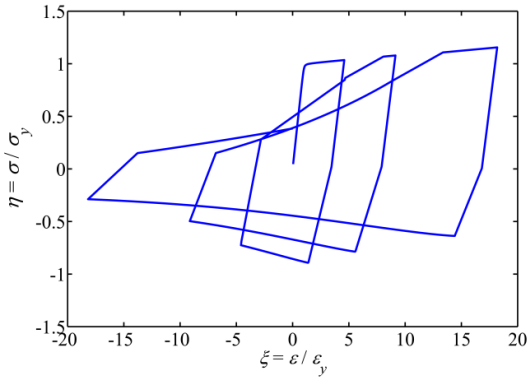

Fig. 6 Cyclic response of *CorrodedReinforcingSteel* material model without corrosion

5.2.3. Uniaxial reinforcing steel material model using *Hysteretic* model in the OpenSees

In this section the tension and compression envelope of the *Hysteretic* available in the OpenSees is fitted to *CorrodedReinforcingSteel* model and used in parametric study. This is because, it is very difficult to change the cyclic rules and pinching parameters of the *CorrodedReinforcingSteel* model by changing the implemented C^{++} code in the OpenSees in parametric study. Therefore, to find the optimum pinch parameters the *Hysteretic* model is used in the parametric study.

The uniaxial *Hysteretic* material model in the OpenSees is a generic hysteric model that can be used to model stress-strain behaviour of a material or force-displacement behaviour of a structural component. The backbone curves in tension and compression can be defined by three points. The cyclic response is defined by two pinch parameters that need to be calibrated for the proposed material or structural component. In this research the *Hysteretic* model is used in parametric study to calibrate the buckling parameters of the new Kashani's buckling model (*CorrodedReinforcingSteel*) [28,29].

The post-buckling envelope of *CorrodedReinforcingSteel* is very similar to Dhakal-Maekawa buckling model [17]. The only difference is that Dhakal-Maekawa model defines the post-buckling response with a three point trilinear curve and *CorrodedReinforcingSteel* defines the post-buckling response using a smooth exponential function. The main differences between the two models are the cyclic rules including pinching effect, fatigue degradation and corrosion effect.

Fig. 7(a) shows a comparison between the buckling envelope of the adopted *Hysteretic* material model and the *CorrodedReinforcingSteel* material model and Fig 7(b) shows an example of the cyclic response of the *Hysteretic* material model. Further details and the influence of pinching parameters on the cyclic rules of *Hysteretic* model are discussed in the parametric study section.

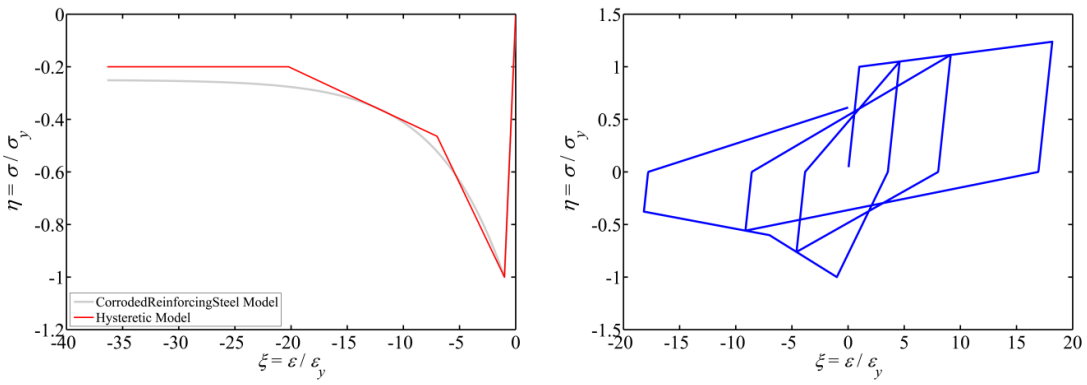

(a) **(b)**

Fig. 7 Cyclic response of *Hysteretic* material model: (a) buckling envelope (b) cyclic response

5.3. Low-cycle fatigue degradation model

OpenSees has a generic fatigue material model that can be wrapped to any steel model without changing the stress-strain state of the parent material. This material model accounts for the effect of low-cycle fatigue and is known as uniaxial *Fatigue* material model in the OpenSees. The model employs a modified rain-flow cycle counter to track strain amplitudes [48]. The

cycle counter is used in conjunction with Coffin-Manson relationship (Eq. (6)) and Miner's Rule to describe the low-cycle fatigue failure [49,50].

$$\varepsilon_p = \varepsilon_f \left(2N_f\right)^{-\alpha} \tag{6}$$

where, ε_p is the plastic strain amplitude ($\varepsilon_p = \varepsilon_a - \varepsilon_e$ where, ε_a is the total strain amplitude and ε_e is the elastic strain), $2N_f$ is the number of half-cycles to failure and α and ε_f are material constants [51,52].

The material constants α and ε_f are the input parameters in the *Fatigue* model. By wrapping this model to any steel model, once the *Fatigue* material reaches a damage state of 1.0, the stress of the parent material becomes zero. An example graph of the *Fatigue* material model wrapped to *Steel02* is shown in Fig. 8.

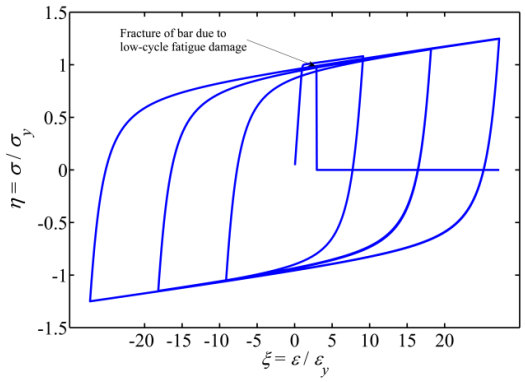

Fig. 8 Fatigue material model to predicting the fracture of reinforcement due to low-cycle fatigue.

5.4. Bond-slip displacement model for zero length element

5.4.1. Tensile stress-slip model for reinforcing steel

In seismic design of RC bridge piers, plastic hinges are designed to form at the column ends (column to foundation/capping beam connection). This will result in slippage of longitudinal bars due to the substantial strain penetration along the bars into the foundation. This phenomenon has been observed by several researchers who studied the cyclic behaviour of RC columns experimentally [33]. Lowes and Altoontash [53] developed a bar-slip model for the end slip of longitudinal reinforcement in beam-column joints as shown in Fig. 9. Using the model in Fig. 9 the bar stress-slip relationship can be calculated using the Eqs. (7) to (11).

$$slip = \int_0^{l_{\sigma_s}} \tau_e \frac{\pi d_b}{A_b} \frac{1}{E} x \, \mathrm{d}x \Rightarrow slip = \frac{2\tau_e l_{\sigma_s}^2}{E\, d_b} \qquad \forall \quad \sigma_s < \sigma_y \tag{7}$$

$$slip = \int_0^{l_e} \frac{4\tau_e}{d_b}\frac{1}{E}x\,\mathrm{d}x + \int_{l_e}^{l_e+l_y}\left(\frac{\sigma_y}{E} + \tau_y\frac{4\left(x-l_e\right)}{d_b E}\right)\mathrm{d}x \qquad \forall \quad \sigma_s > \sigma_y$$
$$\Rightarrow slip = 2\frac{\tau_e l_e^2}{E\ d_b} + \frac{\sigma_y l_y}{E} + \frac{\tau_y l_y^2}{E_h d_b} \tag{8}$$

$$l_{\sigma_s} = \frac{\sigma_s}{\tau_e}\cdot\frac{A_b}{\pi d_b} \tag{9}$$

$$l_e = \frac{\sigma_y}{\tau_e}\cdot\frac{A_b}{\pi d_b} \tag{10}$$

$$l_y = \frac{\sigma_s - \sigma_y}{\tau_y}\cdot\frac{A_b}{\pi d_b} \tag{11}$$

where, σ_s is bar stress at the column-foundation perimeter; σ_y is yield strength of reinforcing bar; E is steel elastic modulus; E_h is steel hardening modulus assuming a bilinear stress–strain response; τ_e is bond strength for elastic steel; τ_y is bond strength for yielded steel; A_b is nominal bar cross section area; and d_b is nominal bar diameter and l_e and l_y, are the lengths along the reinforcing bar for which steel stress is less than and greater than the yield stress respectively.

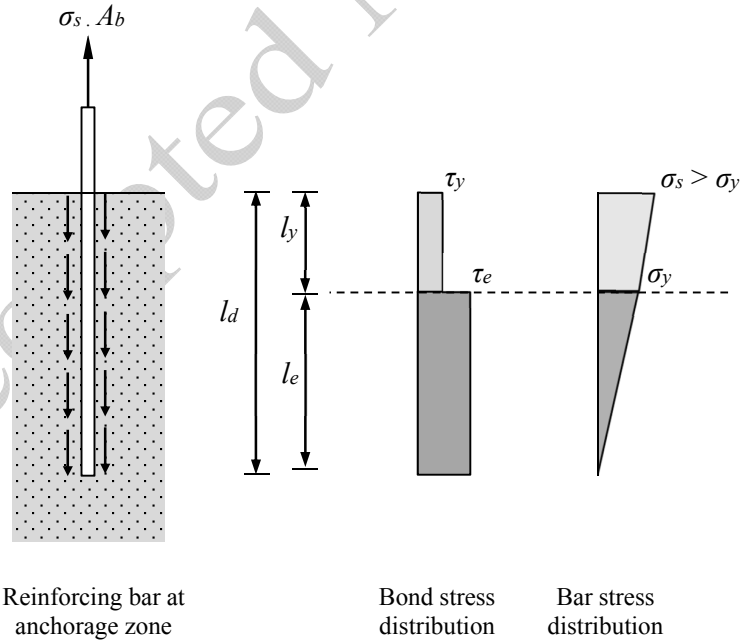

Fig. 9 Bar slip model [52]

Berry and Eberhard [36] conducted a comprehensive parametric study and provide recommendations for the values of bond strength to be used in modelling RC columns. The

suggested values of average bond strengths are summarised in Table 3. The suggested value of steel hardening ratio (E_h/E) is suggested to be taken as 0.1.

Table 3 Average bond strength as a function of steel stress state

Bars stress	Average bond strength (σ_c^* in MPa)
$\sigma_s \leq \sigma_y$	$0.9\sqrt{\sigma_c}$
$\sigma_s > \sigma_y$	$0.45\sqrt{\sigma_c}$

* σ_c is the compressive strength of concrete

The material parameters of the *Steel02* are modified using the Eqs. (5) to (9) and used to model the bar stress-slip behaviourFig. 10 shows the normalised cyclic bar stress-slip response of the model that is used in this study. The S_y in Fig. 10 is the slip at onset of yielding of reinforcement.

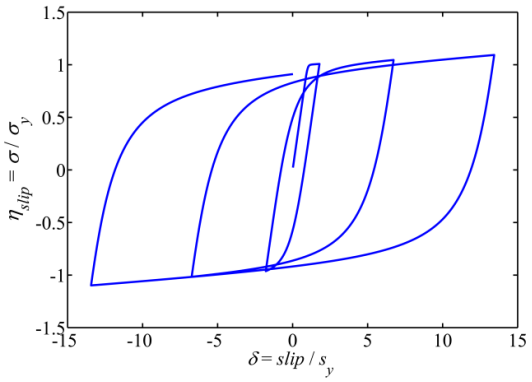

Fig. 10 Bar stress-slip model used in zero length section

5.4.2. Compressive stress-slip model for concrete

The slippage of longitudinal bars in tension combined with the compression due to flexure and axial force results in a highly localised compressive stress in concrete in compression zone. This will cause a localised damage in confined concrete over a so-called d_{comp} depth [36] as shown in Fig. 11.

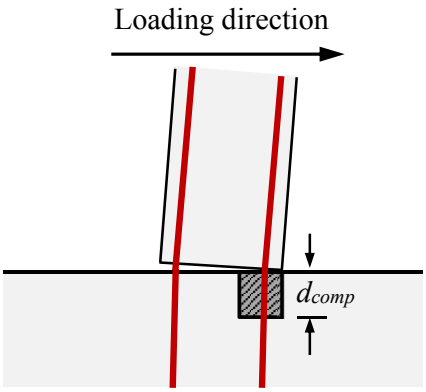

Fig. 11 Assumed compressive depth [36]

[36] recommended the value of d_{ecomp} to be $0.5c$ where c is the depth of neutral axis. In this study $d_{comp} = 0.3D$ is used in the analyses where D is the column diameter.

The uniaxial material *Concrete01* available in the OpenSees (concrete model with zero tension) is used to model the concrete in zero length section. The *Concrete04* has more parameters including tension branch. Changing these parameter and setting the tension branch of the *Concrete04* to zero resulted in numerical instability. Therefore, a simpler model is used in the zero length section element. The stress-strain behaviour of this model is modified by multiplying the strain by d_{comp}. It should be noted that the whole zero length section was considered to be confined concrete. The confinement parameters are the same parameters as the concrete model used in the column. However, given the zero length section element is extremely confined in the foundation it was assumed that the post-peak branch of the concrete model deteriorates up to 80% of the maximum compressive strength of the confined concrete and then follows a perfectly plastic plateau [54]. The stress-slip model of confined concrete model used in zero length section is shown in Fig. 12.

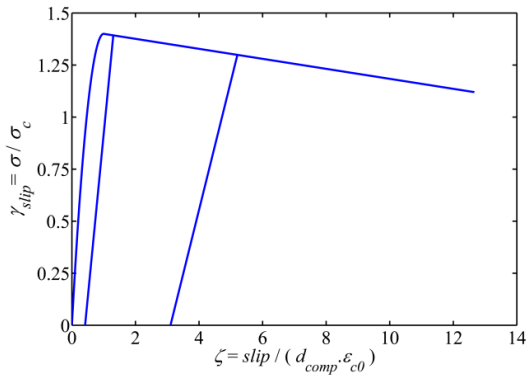

Fig. 12 concrete stress-slip model used in zero length section

6. Initial analysis and comparison of the *Steel02* and the new *CorrodedReinforcingSteel* material models before calibration

The main objective of this research is to investigate the influence of buckling and low-cycle fatigue degradation of vertical reinforcement on the nonlinear cyclic response of RC columns. Therefore, the material models for concrete and zero length element are kept unchanged throughout the analyses based on the recommendations suggested by [36].

To validate the basic model, the computed responses of the proposed fibre model using *Steel02* material model are compared with the experimental results (Fig. 13).

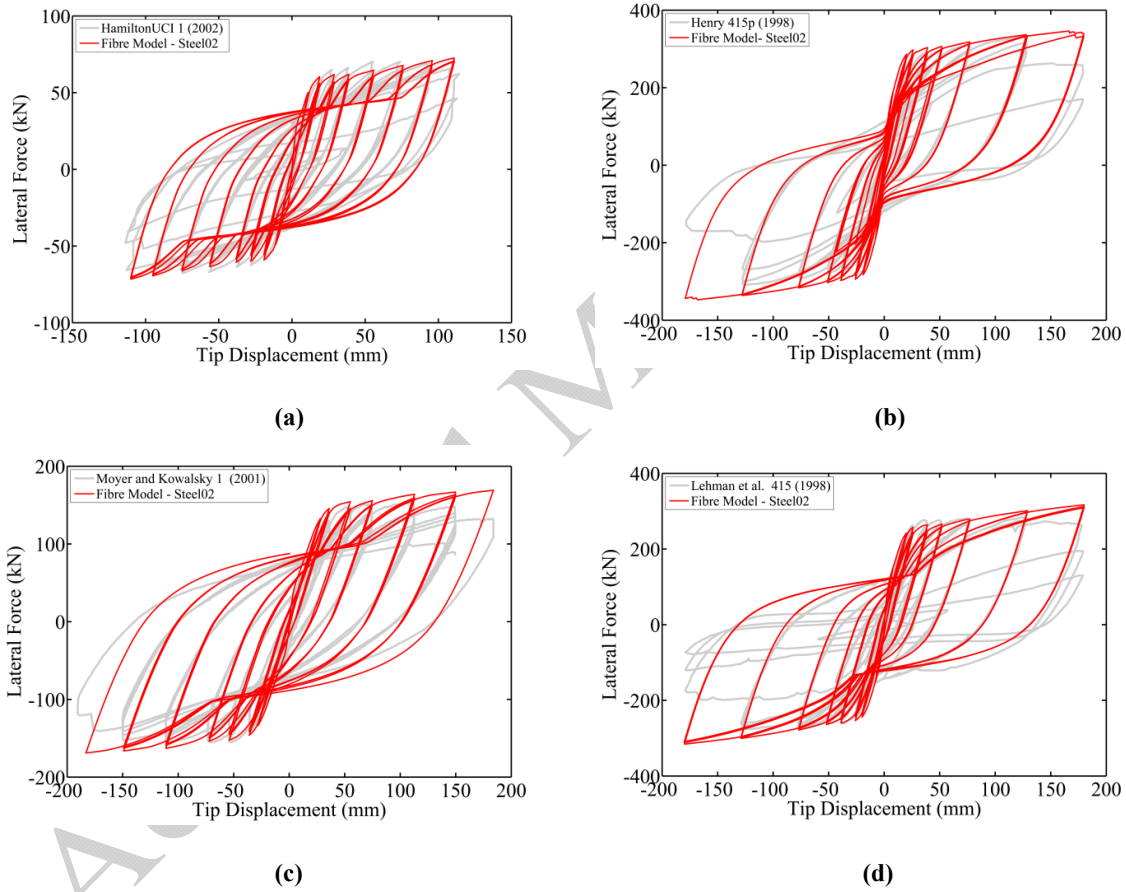

Fig. 13 Examples of computed force-displacement responses of the RC columns using *Steel02* material model

The computed responses in Fig. 13 are identical to those computed by [36]. The *Steel02* can predict the cyclic response of columns accurately until the point that strength degradation starts. This is due to the effect of inelastic buckling and low-cycle fatigue degradation of vertical reinforcement. The effect of strength degradation is less significant in columns that the effective buckling length of vertical reinforcement is relatively small (e.g. Fig. 13 (c) with $L_{eff} / d = 4$).

In the second run, the *Steel02* model is replaced with the new *CorrodedReinforcingSteel* that includes inelastic buckling and low-cycle fatigue degradation. The buckling lengths used in the model are the computed values using Dhakal-Maekawa methodology [16] (as summarised in Table 2). The fatigue parameters are taken based on the recommended values reported by [51]. It should be noted that both buckling and fatigue parameters are calibrated for isolated bars and the model is not calibrate for bars inside RC columns at this stage. Fig. 14 shows two examples of the computed responses using uncalibrated *CorrodedReinforcingSteel* considering no corrosion.

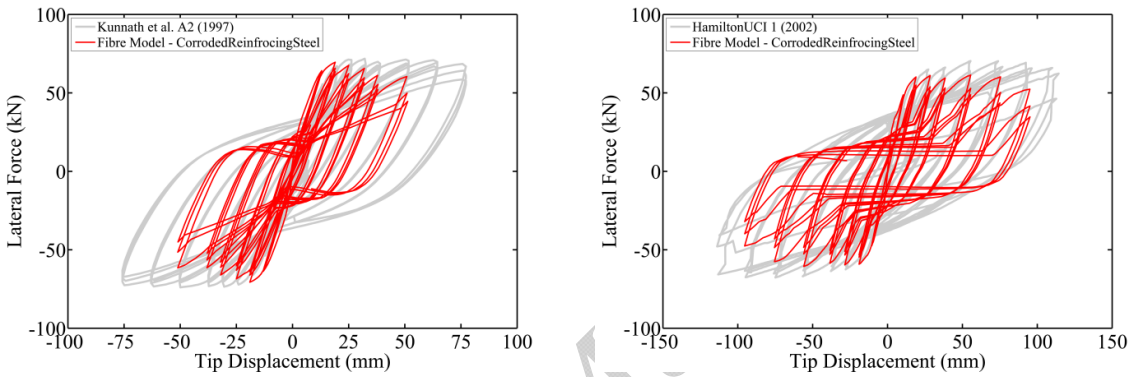

(a) **(b)**

Fig. 14 Examples of force-displacement responses using *CorrodedReinforcingSteel* model

It is clear from the Fig. 14 that computed responses using the new *CorrodedReinforcingSteel* material model are significantly different from the observed experimental responses. As expected, the buckling model of reinforcing bars calibrated using stress-strain behaviour of isolated bars (bare bar) is not representing the real behaviour of reinforcing bars inside the concrete. Dhakal-Maekawa methodology can accurately predict the buckling length of vertical bars. However, for a given buckling length, the lateral deformation (after buckling) of an isolated bar is more than the same bar inside concrete. Therefore, when a material model based on the behaviour of isolated bars is used in the fibre model, it unrealistically increases the compression strain demand at the critical section. As a result, core confined concrete crushes very early, and so the whole model becomes unstable quickly. The comparison of the numerical and experimental shows that the stiffness of horizontal ties are not only affecting the buckling mode and length but also affecting the cyclic stress-strain behaviour of bars. In other words the interaction of horizontal tie reinforcement and vertical reinforcement under cyclic loading must be considered in the cyclic rules of the reinforcing steel.

The previous experimental and numerical studies on the nonlinear cyclic response of reinforcing bars showed that buckling results in a severe pinching effect in cyclic response of isolated reinforcing bars [20,28,29,55]. This effect is due to the influence of geometrical nonlinearity on stress-strain behaviour of isolated bars. However, when reinforcing bars are inside the concrete and restrained by horizontal ties, the cyclic response and strength degradation of bars are influenced by tie stiffness. Therefore, the pinching effect in cyclic response of reinforcing bars inside the concrete is not as severe as the isolated bars.

Solving this problem is a very challenging task, because the *CorrodedReinforcingSteel* is modelling three phenomena in one uniaxial material models. These phenomena are due to material plasticity, geometrical nonlinearity caused by buckling and low-cycle fatigue degradation. Accordingly, a parametric study is conducted to find an optimum uniaxial material model for vertical reinforcing bars that provides an accurate prediction of the cyclic response of RC columns considering the inelastic buckling of vertical bars. The procedure of the parametric study is discussed in section 7.

7. Parametric study using *Hysteretic* material model

7.1. Selection of pinching parameters

The *Hysteretic* material model in the OpenSees has two pinching parameters (pinch *x* and pinch *y*). Pinch *x* is the pinching factor for strain, ranging from 0 to 1 and pinch *y* is the pinching factor for stress, ranging from 0 to 1. Using these parameters it is possible to control the pinching response of the material model. In the current parametric study, nine combinations which are representing three types of pinching responses are considered (Fig. 15). The pinching combinations used in the parametric study are summarised in Table 4.

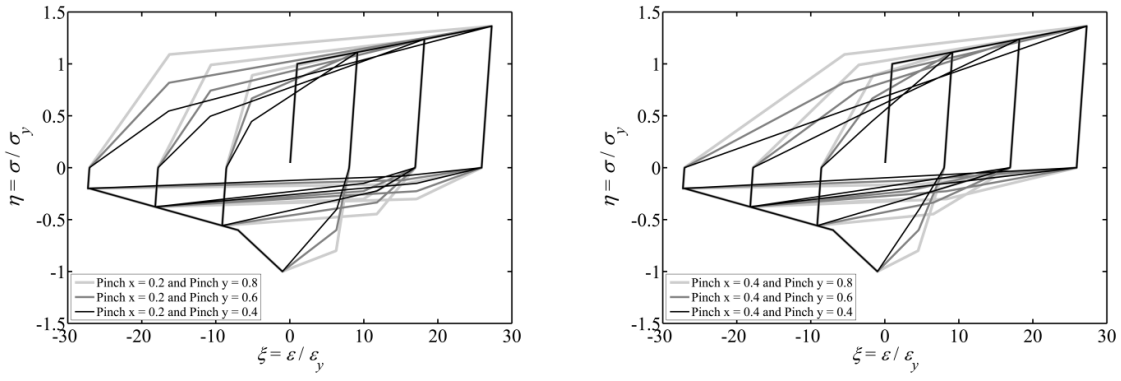

(a) **(b)**

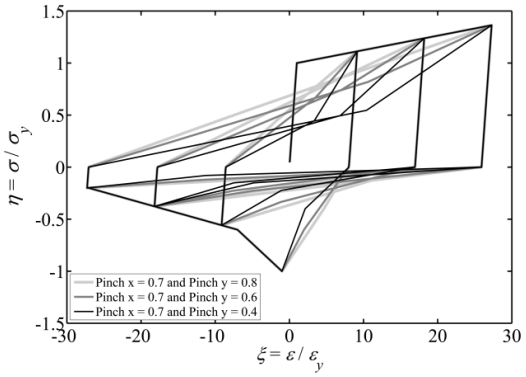

(c)

Fig. 15 Cyclic responses of reinforcing bar using *Hysteretic* material model with L_{eff}/d = 10 and different pinching parameters: (a) small pinch (b) moderate pinch (c) severe pinch

Table 4 Pinch combination used in the parametric study

Combination	**1**	**2**	**3**	**4**	**5**	**6**	**7**	**8**	**9**
pinch *x*	0.2	0.2	0.2	0.4	0.4	0.4	0.7	0.7	0.7
pinch *y*	0.8	0.6	0.4	0.8	0.6	0.4	0.8	0.6	0.4

The error in hysteretic energy dissipation (Eq. (11)) is used as a measure of accuracy in the parametric study.

$$\Omega_E = \frac{\left|E_{meas} - E_{comp}\right|}{E_{meas}} \tag{12}$$

where, Ω_E is the energy error, E_{meas} is the measured dissipated energy in experiment and E_{comp} is the computed dissipated energy in fibre model.

It should be noted that for calculation of the dissipated hysteretic energy only hysteretic cycles before severe strength loss in the cyclic response are considered. In this study, when the column strength falls below 80% of the maximum strength, it is considered as severe strength loss and is identified as the maximum drift capacity. It should be noted that the low-cycle fatigue is not considered in the parametric study.

7.2. Comparison of the hysteretic energy dissipation

Fig. 16 shows the Ω_E of each column test experiment for all the pinching parameters. It is clear from Fig. 16 that the error in pinching combination number 1 to 4 and number 8 to 10 are quite big. However, the error in combination number 5 to 7 is normally below 10% for most columns. It was found that among these three combinations, the combination 6 has the smallest average error in predicted response. As mentioned earlier, the pinching response of the reinforcing bars

is affected by the spacing horizontal tie reinforcement (s/d). Moreover, the cyclic response of the RC columns is also affected by axial force ratio and ratio of vertical reinforcement (ρ_l). Therefore, the correlation between the pinch parameters (pinch x and pinch y) and ρ_l, s/d and axial force ratio is investigated. It was found that there is not any correlation between these parameters. This is because there is not enough variation in ρ_l, s/d and axial force ratio in the experimental dataset. Therefore combination 6 is taken as the optimum model for further analyses.

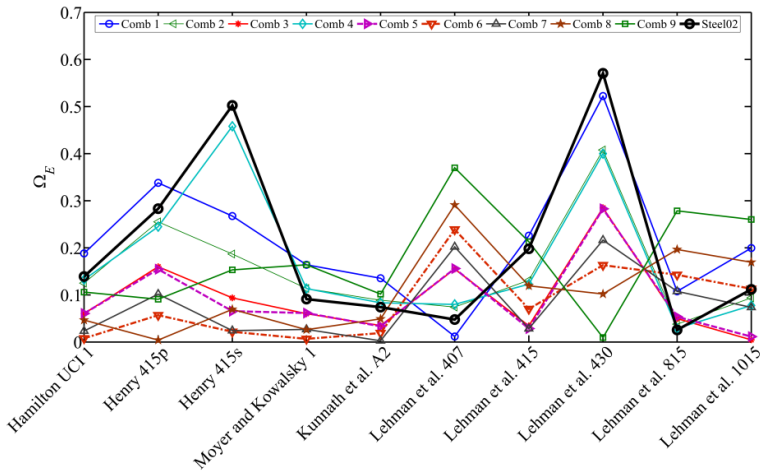

Fig. 16 Error in hysteretic energy dissipation of each pinch combination for all the columns

8. Discussion of computational results of the optimised model

8.1. Discussion of results of buckling included model without the low-cycle fatigue

Fig. 17 shows the qualitative comparison of the OpenSees model with optimised uniaxial material model (the *Hysteretic* model fitted to *CorrodedReinforcingSteel* model) of reinforcement with the effect of buckling and the experimental dataset.

It is clear from the Fig. 17 that the predicted responses of the optimised model are in a very good agreement with observed experimental responses. For example consider the Fig. 17(a) and (b) which shows the Henry's columns 415p and 415s. All the details of these two columns are identical apart from the s/d. The difference in s/d resulted in a change in buckling length. Therefore, the response of column 415p with L_{eff}/d = 10 is more pinched compare to the response of column 415s with L_{eff}/d = 8. This observation is consistent with the observed experimental response.

The buckling of vertical bars in columns results in strength loss in post-buckling branch of stress-strain response of reinforcement. This strength loss in reinforcing steel increases the stress in core confined concrete. Moreover, the core expansion and the horizontal deformation of vertical bars due to buckling results in yielding and subsequently fractures of horizontal tie reinforcement. In these circular column the failure mode is found to be bar buckling and then followed by gradual core concrete crushing. This is due to the geometry of the column cross section and might be different in rectangular cross sections. As a result the core confined concrete crushes much sooner than a situation where buckling is not an issue or buckling length is short ($L_{eff}/d < 6$). This mechanism causes a severe loss of strength that degrades during the cyclic loading of column. This can be clearly seen in Fig. 17. By comparing the computational responses using *Steel02* and the optimised buckling model, it is apparent that the strength degradation cannot be captured using *Steel02*.

It was observed that if vertical bars buckle over a short length the buckling of vertical bars doesn't have a significant influence on cyclic response of the column. This has been shown previously in Fig. 13(c) (Moyer and Kowalsky's column 1). Vertical reinforcement in this column buckled over one tie spacing, therefore $L_{eff}/d = s/d = 4$. In this case, the numerical responses using *Steel02* is in a very good agreement with the observed experimental response. This can be seen in Fig 16 where the error in the dissipate energy using *Steel02* is very small and is very similar to *Hysteretic* model. [19,28,29,55] reported that for ordinary high yield reinforcing bars with yield strength ranging from 400MPa to 500MPa, if the $L_{eff}/d < 6$, the postbuckling response in compression is almost identical to the tension envelope and buckling doesn't significantly influence the cyclic stress-strain behaviour of reinforcement. Moreover, given the buckling length is very short, the horizontal deformation is smaller than bars with larger buckling lengths. Therefore, horizontal tie reinforcement are not quickly fractured following the buckling of vertical bars. As a result the column can sustain a much larger drift without crushing of core confined concrete in compression.

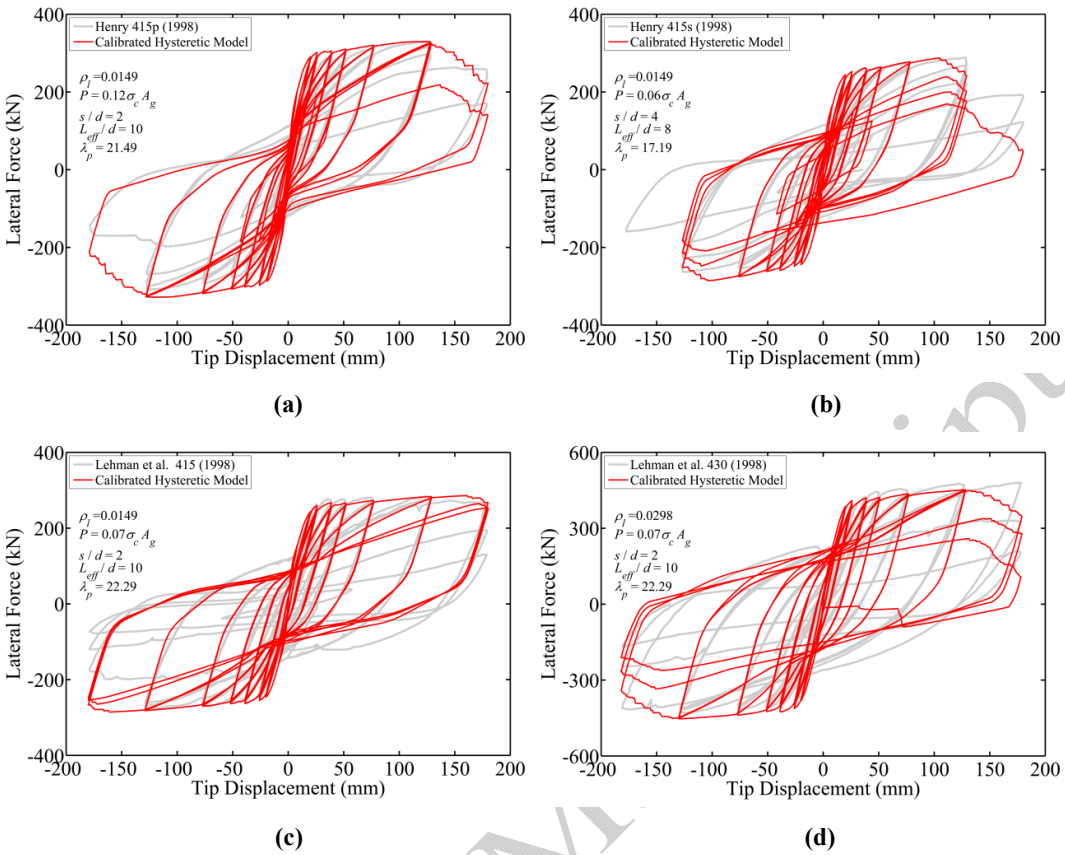

Fig. 17 Force-displacement responses for the experimental dataset using calibrated *Hysteretic* model

In order to quantify the accuracy of the numerical model the error in predicting the response at critical stages are compared (Eq. (13)). The considered stages are the initial stiffness ($K_{initial} = F_y/\Delta_y$ where the F_y is the force at first yield of reinforcement and Δ_y is the corresponding displacement), prediction of the 1% drift capacity (F_1) and the prediction of the maximum drift capacity (F_{max}). The F_{max} is the force at the maximum drift, that column experienced in the physical test. Table 5 shows the results of this comparison including the statistics of the error data.

$$\Psi_{\eta} = \left| \frac{\eta_{experiment} - \eta_{computed}}{\eta_{experiment}} \right| \tag{13}$$

Where, $\eta_{experiment}$ is the experimental value of the considered variable ($K_{initial}$, F_1 and F_{max}) and $\eta_{computed}$ is the computed predicted value of the considered variable ($K_{initial}$, F_1 and F_{max}).

Table 5 Quantitative comparison of the error in the optimised model and experimental dataset

Experiment	$\Psi_{Kinitial}$	Ψ_{F1}	Ψ_{Fmax}
Kunnath et al. A2 [31]	0.236	0.175	0.083
Lehman and Moehle 415 [32]	0.059	0.012	0.004

Lehman and Moehle 815 [32]	0.131	0.132	0.167
Lehman and Moehle 1015 [32]	0.246	0.295	0.222
Lehman and Moehle 407 [32]	0.018	0.011	0.029
Lehman and Moehle 430 [32]	0.260	0.188	0.038
Henry 415p [32]	0.404	0.169	0.000
Henry 415s [32]	0.366	0.110	0.120
Moyer and Kowalsky 1[33]	0.275	0.268	0.245
Hamilton UCI1 [34]	0.238	0.045	0.127
Mean Value	0.223	0.140	0.104
Standard Deviation	0.117	0.094	0.084
Max	0.404	0.295	0.245
Min	0.018	0.011	0.000

8.2. Discussion of results of buckling included model combined with low-cycle fatigue

The observed experimental results show that some of the columns experienced bar fracture in tension shortly after buckling. The point at which bar fracture occurred during the cyclic test for each column is reported in the relevant references. In this research the *Fatigue* model in the OpenSees is wrapped to the optimised buckling model to model the fracture of bars due to low-cycle fatigue. The fatigue material constants (α and ε_f) are set to predict the bar fracture at the same point as is observed in the experiment. Fig. 18 shows example of cyclic responses considering the fracture of reinforcing bars due to fatigue.

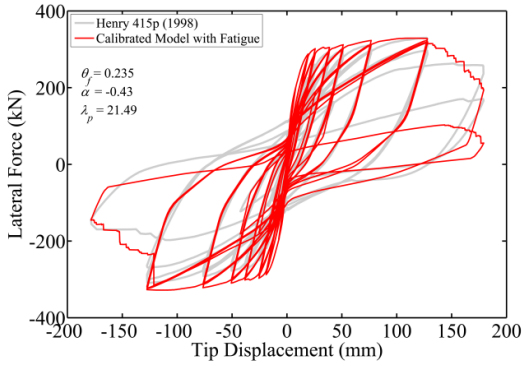

(a)

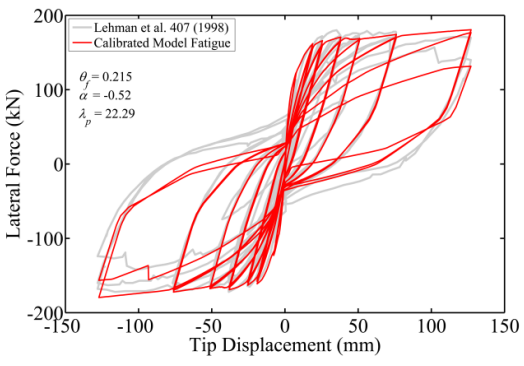

(b)

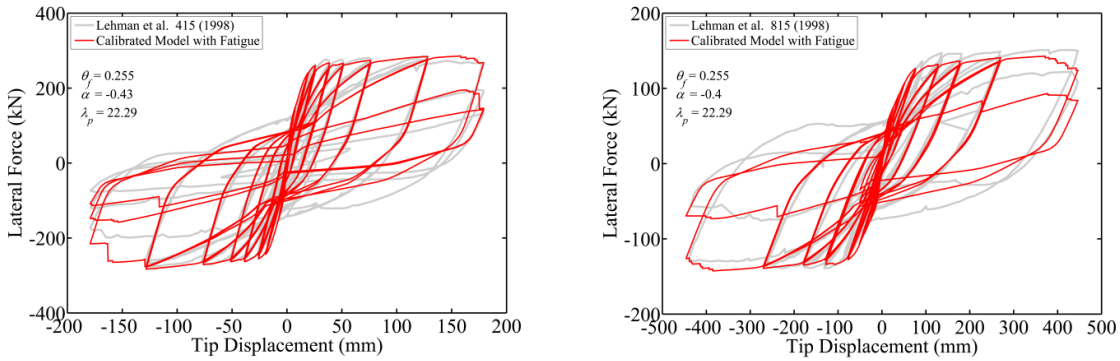

(c) **(d)**

Fig. 18 Force-displacement responses for the experimental dataset using calibrated *Hysteretic* model combined with *Fatigue* model

It was found that the fracture of bars in tension and fatigue material constants are sensitive to λ_p. All the Columns with λ_p < 18 didn't experience bar fracture in tension. However, as λ_p increased the low-cycle fatigue life of bars reduced. This shows that the low-cycle fatigue life of reinforcing bars is a function of compound non-dimensional slenderness ratio λ_p. This can be shown by comparing Henry's column 415p with λ_p = 21.49 and 415s with λ_p = 17.19. Fig. 18(a) shows the response of Henry's column 415p that experienced bar fracture in tension. However, bar fracture in tension was not observed in Henry's column 415s as shown in Fig. 17(b). This is in a good agreement with the experimental results reported by [56,57].

This shows that the combined effect of inelastic buckling and low-cycle fatigue degradation has a significant influence on inelastic response of RC columns. Fig. 19 shows a comparison between the normalised accumulated energy dissipation in two columns. It should be noted that the dissipated energy in Fig. 19 is normalised to the dissipated energy under elastic region of the monotonic pushover curve. Fig. 19(a) shows the Henry's column 415p with λ_p = 21.49 and Fig. 19(b) shows Moyer and Kowalsky's column 1 with λ_p = 9.5.

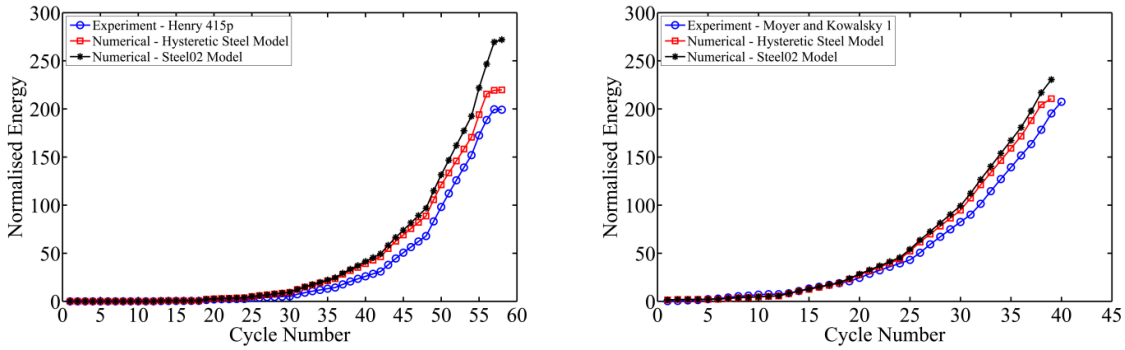

Fig. 19 Influence of material model on accumulated energy dissipation: (a) Henry 415p and (b) Moyer and Kowalsky 1

Fig. 19(a) shows that as the number of cycles increase there is a cumulative error in the numerical model with *Steel02*. However, Fig. 19(b) shows that the predicted response using *Steel02* and the optimised buckling model with fatigue is almost identical. This is another argument which suggests that the bar buckling parameter, λ_p, has a significant influence on the inelastic response of RC columns. This is an area for further research to develop a methodology to calibrate the fatigue material constants as a function of λ_p.

For further validation of the calibrated model a set of cyclic analysis on Kunnath et al. [32] columns with random displacement history is conducted. These columns were not included in the calibration process. Fig. 20 shows the comparison of the simulated and experimental results of column A11. Fig. 20 (a) shows the simulated response using calibrated buckling model without considering fatigue and Fig. 20 (b) shows the simulated response using calibrated buckling model combined with fatigue model. It is evident from the Fig. 20 that the calibrated model is capable of predicting the inelastic response of RC columns under arbitrary random load history. Moreover, the model is able to account for cyclic degradation due to combined effect of buckling and low-cycle fatigue degradation of vertical reinforcement.

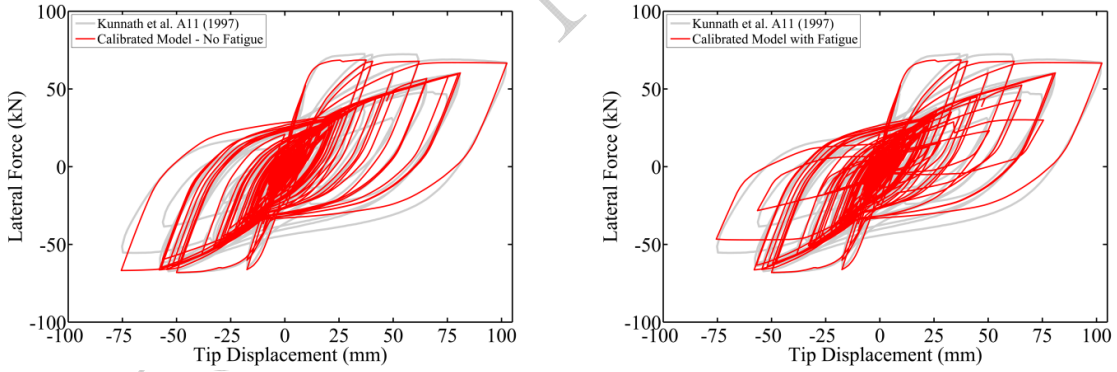

(a) **(b)**

Fig. 20 Force-displacement responses for Kunnath et al column A11 under earthquake loading pattern: (a) calibrated buckling model without considering fatigue (b) calibrated buckling model with fatigue

9. Conclusion

A new modelling technique for nonlinear analysis of RC bridge piers considering the inelastic buckling and low-cycle fatigue of vertical reinforcing bars is developed. The numerical model is calibrated using UW-PEER experimental RC column dataset. The main conclusions and outcomes of this research can be summarised as below:

1. The localisation issue in force-based elements in structural systems with softening response due to buckling can be resolved by using two elements. As suggested the integration length of the first section of first element must be taken the same as the buckling length considered in the uniaxial material model of reinforcing steel.
2. The methodology developed by [16] for calculation of buckling length showed a very good agreement with the observed experimental results of circular columns. Therefore, it can be used as a reliable model in calculation of the buckling length of reinforcing bars in RC columns accounting for the stiffness of horizontal tie reinforcement.
3. It was found that the new uniaxial material model for reinforcing bars that developed and implemented in OpenSees by [28] cannot represent the cyclic behaviour of reinforcing bars inside concrete. This is because the model is calibrated using the experimental and numerical data of isolated bars and doesn't account for the influence of horizontal tie reinforcement. Such an enhancement to the bar material model, that fully accounts for the influence of tie reinforcement, is an area for future research.
4. The observed experimental and numerical results showed that fracture of bars due to low-cycle fatigue is very sensitive to the compound non-dimensional slenderness ratio of bars (λ_p). This is an area for future research..
5. The final calibrated model (*Hysteretic* material model) has identical backbone curves in tension and compression (buckling curve) to *CorrodedReinfrocingSteel*. This calibrated model has optimum pinch parameters (pinch *x* and pinch *y*) that were calibrated in the parametric study. The results show a very good agreement in predicting the nonlinear cyclic response of circular RC columns using this optimised model. The model is also validated against column experiments with random displacement history which were not included in calibration process. Although there is need for further model calibration, nevertheless the modelling technique developed in this paper can be used in nonlinear seismic analysis and evaluation of RC bridges as a reliable tool for both researchers and practicing engineers.

Acknowledgement

This research is conducted by collaboration of the University of Bristol with the University of Washington while the first author was on sabbatical leave in the US. The funding provided by the World Wide University Network through Research Mobility Programme to the first author is much appreciated. Authors would like to thank Prof. Marc O. Eberhard and Prof. John F.

Stanton for providing valuable guidance during the course of this research. Any findings, opinions and recommendations provided in this paper are only based on the author's view.

References

[1] Berry M, Eberhard MO. Performance Models for Flexural Damage in Reinforced Concrete Columns. Pacific Earthquake Engineering Research Centre, Research Report, University of California Berkeley 2003; 162.

[2] Lehman DE, Moehle JP, Mahin SA, Calderone AC, Henry H. Experimental valuation of Seismic Design Provisions for Circular Reinforced Concrete Columns. J Struct Eng 2004; 130 (6): 869-879.

[3] Berry MP, Eberhard MO. Practical performance model for bar buckling." J Struct Eng 2005; 131 (7): 1060-1070.

[4] Taucer F, Spacone E, Filippou FC. A fibre beam-column element for seismic response analysis of reinforced concrete structures. EERC College of Engineering, University of California 1991; 91 (17).

[5] Spacone E, Filippou FC, Taucer FF. Fibre beam-column model for non-linear analysis of R/C frames: Part I. Earthq Eng Struct D 1996; 25(7): 711-726.

[6] Spacone E, Filippou FC, Taucer FF. Fibre beam-column model for non-linear analysis of R/C frames: Part II. Applications. Earthq Eng Struct D 1996; 25(7): 727-742.

[7] Pantazopoulou SJ Detailing for reinforcement stability in reinforced concrete members. J Struct Eng 1998; 124(6): 623–632.

[8] Papia M, Russo G. Compressive concrete strain at buckling of longitudinal reinforcement. J Struct Eng 1989; 115(2): 382–397.

[9] Papia M, Gaetano R, Gaetano Z. Instability of longitudinal bars in RC columns. J Struct Eng 1988; 114 (2): 445–461.

[10] Monti G, Nuti C. Nonlinear cyclic behaviour of reinforcing bars including buckling J Struct Eng 1992; 118 (12): 3268–3284.

[11] Mau ST, El-Mabsout M. Inelastic buckling of reinforcing bars J Eng Mech 1989; 115(1): 1–17.

[12] Mau ST. Effect of tie spacing on inelastic buckling of reinforcing bars ACI Struct J 1990; 87(6): 671–678.

[13] Rodriguez ME, Botero J, C, Villa J Cyclic stress-strain behaviour of reinforcing steel including the effect of buckling. J Struct Eng 1999; 125 (6): 605–612.

[14] Scribner CF. Reinforcement buckling in reinforced concrete flexural members. ACI J 1986; 83(6): 966–973.

[15] Gomes A, Appleton J Nonlinear cyclic stress-strain relationship of reinforcing bars including buckling. Eng Struct 1997; 19: 822–826.

[16] Dhakal RP, Maekawa K. Reinforcement stability and fracture of cover concrete in RC members. J of Struct Eng 2002; 128 (10): 1253–1262.

[17] Dhakal RP, Maekawa K. Modeling for postyield buckling of reinforcement. J of Struct Eng 2002; 128 (9): 1139–1147.

[18] Dhakal RP, Maekawa K. Path-dependent cyclic stress-strain relationship of reinforcing bar including buckling. Eng Struct 2002; (24): 1139–1147.

[19] Kashani MM, Crewe AJ, Alexander NA. Nonlinear stress-strain behaviour of corrosion-damaged reinforcing bars including inelastic buckling. Eng Struct 2013; 48: 417–429.

[20] Kashani MM, Crewe AJ, Alexander NA. Nonlinear cyclic response of corrosion-damaged reinforcing bar with the effect of buckling. Constr Build Mater 2013; 41: 388–400.

[21] Kunnath SK, Heo Y, JF Mohle. Nonlinear uniaxial material model for reinforcing steel bars. J Struct Eng 2009; 135 (4): 335–343.

[22] Bae S, Mieses A, Bayrak O. Inelastic buckling of reinforcing bars. J of Struct Eng 2005; 131 (2): 314–321.

[23] Bayrak, O and Sheikh A Shamim. Plastic hinge analysis. J of Struct Eng 2001; 127(9): 10092–1100.

[24] Cosenza E, Prota A. Experimental behavior and numerical modeling of smooth steel bars under compression. J of Earthquake Eng 2006; 10(3): 313-329.

[25] Zong Z, Kunnath S, Monti G. Material Model Incorporating Buckling of Reinforcing Bars in RC Columns. J Struct Eng 2013; 140(1): 04013032(10).

[26] Coleman J, Spacone E. Localisation issues in force-based frame elements." J Struct Eng 2001; 127(11): 1257–1265.

[27] Pugh JS. Numerical simulation of walls and seismic design recommendations for walled buildings. PhD Thesis 2012; University of Washington.

[28] Kashani MM. Seismic performance of corroded RC bridge piers: development of a multi-mechanical nonlinear fibre beam-column model**.** PhD Thesis 2014; University of Bristol.

[29] Kashani, M. M., Lowes, L. N., Crewe, A. J. & Alexander, N. A. (2015), Phenomenological hysteretic model for corroded reinforcing bars including inelastic buckling and low-cycle fatigue degradation. Comput Struct, Accepted eith minor corrections.

[30] OpenSees, the Open System for Earthquake Engineering Simulation, Pacific Earthquake Engineering Research Centre 2011, University of California, Berkeley.

[31] Berry M, Parrish M, Eberhard M. Performance Database User's Manual. PEER, Univ. of Calif. Berkeley 2004; www.ce.washington.edu/~peera1.

[32] Kunnath SK, El-Bahy A, Taylor AW, Stone WC. Cumulative seismic damage of reinforced concrete bridge piers. Technical Report NCEER 1997; 97-0006.

[33] Lehman DE, Moehle JP. Seismic performance of well-confined concrete columns PEER Research Report, Univ. of Calif. Berkeley 2000.

[34] Moyer MJ, Kowalsky MJ Influence of tension strain on buckling of reinforcement in concrete columns, ACI Struct J 2003; 100 (1): 75-85.

[35] Hamilton CH, Pardoen GC, Kazanjy RP. Experimental Testing of Bridge Columns Subjected to Reversed-Cyclic and Pulse-type Loading Histories. Report 2001-03, Civil Engineering Technical Report Series, University of California 2003; pp200.

[36] Berry MP, Eberhard MO Performance modelling strategies for modern reinforced concrete bridge columns. PEER Research Report, Univ. of Calif. Berkeley 2006; 67 (11).

[37] Jansen D, Shah S. Effect of length on compressive strain softening of concrete. J Eng Mech 1997; 123(1): 25–35.

[38] Lee Y, William K. Mechanical properties of concrete in uniaxial compression. ACI Mat. J 1997; 94(6): 457–471.

[39] Abramowitz M, Stegun CA. Handbook of mathematical functions with formulas, graphs, and mathematical tables. Dover, New York 1972; NY, 9th edition.

[40] Timoshenko S, Gere J. Theory of elastic stability. MacGraw-Hill; 1963, p. 163-182.

[41] Popovics S. A numerical approach to the complete stress strain curve for concrete. Cem Concr Res 1988; 3(5): 583-599.

[42] Karsan ID, Jirsa JO. Behaviour of concrete under compressive loading. J Struct Div 1969; 95(ST12).

[43] Mander JB, Priestley MJN, Park RJ. Theoretical stress-strain model for confined concrete. J Struct Eng 1988; 114(8): 1804-1825.

[44] Menegotto M, Pinto PE. Method of analysis of cyclically loaded RC plane frames including changes in geometry and nonelastic behavior of elements under normal force and bending. Preliminary Report IABSE, Zurich 1973; 13: 15–22.

[45] Filippou FC, Popov EP, Bertero VV. Effects of Bond Deterioration on Hysteretic Behaviour of Reinforced Concrete Joints. UCB/EERC, Univ. of Calif. Berkeley 1983; 83-19.

[46] Bauschinger J. Variations in the elastic limit of iron and steel. The J of the Iron and Steel Institute 1887; 12 (1): 442-444.

[47] Dodd LL, Restrepo-Posada JI. Model for predicting cyclic behavior of reinforcing steel. J of Struct Eng 1995; 121 (3): 433–445.

[48] Uriz P. Towards Earthquake Resistant Design of Concentrically Braced Steel Structures. PhD Thesis 2005; Univ. of Calif. Berkeley.

[49] Manson, SS. Fatigue: A complex subject-Some simple approximations. Exp. Mech 1965; 5 (7): 193–226.

[50] Miner MA. Cumulative damage in fatigue. J Appl Mech 1945; 12: A159–A164.

[51] Brown J, Kunnath SK. Low-cycle Fatigue failure of reinforcing steel bars. ACI Mater J 2004; 101(6): 457–466.

[52] Mander JB, Panthaki FD, Kasalanat A. Low-cycle fatigue behaviour of reinforcing steel. J Mater Civil Eng 1994; 6(4): 453–468.

[53] Lowes LN, Altoontash A. Modelling reinforced-concrete beam-column joints subjected to cyclic loading. J Struct Eng 2003; 129(12): 1686-1697.

[54] Zhao J, Sritharan S. Modelling of strain penetration effects in fiber-based analysis of reinforced concrete structures. ACI Struct J 2007; 1042: 133–141.

[55] Kashani MM, Lowes LN, Crewe AJ, Alexander NA. Finite element investigation of the influence of corrosion pattern on inelastic buckling and cyclic response of corroded reinforcing bars. Eng Struct 2014; 75: 113-125.

[56] Restrepo-Posada JI, Park R, Buchanan AH. Seismic behaviour of connections between precast concrete elements. Res. Rep., 1993: 93-3, Dept. of Civil Engineering, University of Canterbury, Christchurch. New Zealand.

[57] Kashani MM, Barmi AK, Malinova VS. Influence of inelastic buckling on low-cycle fatigue degradation of reinforcing bars. Constr Build Mater 2015; 94: 644-655.